Turk J Phys
27 (2003) , 395 – 417.
© TÜBİTAK

Persistent Currents in Mesoscopic Loops and Networks

Igor O. KULIK
Department of Physics, Bilkent University, Ankara 06533, TURKEY

Received 28.08.2003

Abstract

The paper describes persistent (also termed "permanent", or "non-decaying") currents in mesoscopic metallic and macromolecular rings, cylinders and networks. The current arises as a response of system to Aharonov-Bohm flux threading the conducting loop and does not require external voltage to support the current. Magnitude of the current is periodic function of magnetic flux with a period of normal-metal flux quantum $\Phi_0 = hc/e$. Spontaneous persistent currents arise in regular macromolecular structure without the Aharonov-Bohm flux provided the azimuthal periodicity of the ring is insured by strong coupling to periodic background (a "substrate"), otherwise the system will undergo the Peierls transition arrested at certain flux value smaller than Φ_0. Extremely small (nanoscopic, macromolecular) loop with three localization sites at flux $\Phi = \Phi_0/2$ develops a Λ-shaped energy configuration suitable to serve as a qubit, as well as at the same time as a "qugate" (quantum logic gate) supporting full set of quantum transitions required for universal quantum computation. The difference of the Aharonov-Bohm qubit from another suggested condensed-matter quantum computational tools is in the radiation free couplings in a qubit supporting the scalable, long-lived quantum computation.

1. Introduction

It was predicted in 1970 that normal-metallic rings and hollow cylinders support the non-decaying ("persistent") currents [1, 2] in presence of Aharonov-Bohm flux [3] and periodically changing their amplitude as a function of flux without the external source of voltage electromotive force (e.m.f.). It was pointed in [2] that weak scattering or any other source of dissipation does not decay the current. Counterintuitively, the current is *finite* at zero temperature rather than infinite as it may be deduced from the naive idea of infinite conductivity in the ideal periodic system. Rather, a d.c. conductivity of double connected mesoscopic conductor is *zero* at non zero e.m.f., and has certain critical value at $V_{\text{d.c.}} = 0$ decreasing with the increasing scattering and temperature. Buttiker, Imry, and Landauer [4] further supported this conclusion by considering the impure metal, and showed the equivalence of the arbitrary impure ring of length L to the periodic one-dimensional structure of period L. This paper drived experimental investigations in, at that time ready, mesoscopic physics resulted in a direct detection of persistent currents in metallic [5] and semiconducting [6] rings. In a paper [7], periodic variation of magnetization with magnetic field in macromolecular structure was observed which, to our opinion, may be related to Aharonov-Bohm persistent currents. Recently, is was shown by Barone at al. [8] that persistent-current ring with resonantly coupled quantum dots can serve as an element of quantum computer when static electric field is applied perpendicular to magnetic field in the loop. Further, it was shown that persistent current can be excited in an extremely small ("nanoscopic") loop *without* the Aharonov-Bohm flux [9]. These developments will be considered in chapters 3,4.

Actually, the idea of persistent current traces back to the work of Teller [10] who showed that Landau diamagnetism in metals can be interpreted as an effect of orbital currents in a magnetic field. Most clearly this

can be demonstrated if one considers metal as a periodic network of "sites" (centers of electron localization) on atomic or mesoscopic "loops" which can be termed "mesoscopic network". Overall magnetization in mesoscopic network in the low-field limit nicely fits to the estimation of Landau diamagnetic susceptibility $\chi = \frac{1}{3}N(\varepsilon_F)\mu_B^2$ where $N(\varepsilon_F)$ is density of electron states at Fermi energy ε_F and μ_B is the Bohr magneton.

2. Persistent currents in metals

It was generally believed that currents in conductors, in particular in metals, are necessary related to voltages which are driving forces for collective motion of electrons. The only exception is the case of superconductor when due to infinite conductivity of superconductor, current may exist even at zero voltage. This was a prejudice, however. External fields other than the electric field can also produce a stationary permanent currents. In particular, this happens when the magnetic field, or the field of magnetic vector potential, is applied to normal (nonsuperconducting) metal. The current appears without the electrical electromotive force. Equivalently, this is a statement that the magnetization of conductor exists at zero e.m.f. This is a quantum effect, the permanent magnetization (current) in metal in a magnetic field vanishes if the motion of electrons be considered within the classical (Newtonian) mechanics. The proof of the above statement is known as the Van Leeuwen theorem [11].

Classical trajectory of electron in magnetic field is a small circle, the Larmour orbit (Fig.1). At first sight, such motion necessary creates permanent magnetization since circular current of rotating electron J will create a magnetic moment $M = (1/c)JS$ (S is a surface embraced by the current). Nevertheless, the electrons near the surface of metallic sample are moving along the extended orbits bending to surface and performing overall rotation in a direction opposite to that of the "bulk" electrons. Because of much larger embraced area Σ of the trajectory of these electrons, their magnetic moment is as large as sum of magnetic moments of electrons in the bulk. It turns out that these two contributions exactly cancel each other, and total magnetization remains zero. Such cancellation is a direct consequence of the above theorem. There exists a number of phenomena related to quantization of orbital motion, in particular the de Haas-van Alphen and Shubnikov - de Haas effects [12]. Shortly after the Landau paper [13], Teller have shown[10] that the diamagnetism in metal can be interpreted as an effect of orbital electron currents. The currents are flowing near the metallic surface. This permanent current is nevertheless not much sensitive to scattering of electrons since such scattering, in case when the mean free path of electron is larger than the cyclotron (Larmour) radius, only slightly shifts the electron orbits (Fig. 1) and is not crucially related to phase shifts of the electron wave function (the effect known as a finite "phase breaking length" of electron, l_φ).

In quantum mechanics, instead of following the electron trajectory, we solve the Schrödinger equation for the electron wave function and find the current distribution as

$$\mathbf{j} = \frac{ie\hbar}{2m}(\psi^*\nabla\psi - \psi\nabla\psi^*) - \frac{e^2}{mc}\mathbf{A}|\psi|^2 \tag{1}$$

The magnetization related to this current is exactly the Landau diamagnetism. The current in normal metal is not exactly the same thing as the Meissner current in superconductor. Unlike the latter, normal current fluctuates in time and changes temporarily from one piece of metal to another, but the *average* current remains constant and does not decay in time.

With these ideas, I considered [2] in 1970 the case of more complex topology of conducting pathes in metal, the one in which electron trajectory is restricted between two barriers embracing the Aharonov-Bohm flux like in a hollow cylinder (Fig.2), i.e. the double connected metallic sample. Quantum dynamics of electron in a double connected geometry is specified by the Aharonov-Bohm effect. Aharonov and Bohm predicted [3] that double connected geometry makes, quantum mechanically, vector potential $\mathbf{A}$ a physically meaningful quantity rather than pure mathematical abstraction like in case of classical physics in which magnetic field alone $\mathbf{B} = curl\mathbf{A}$ determines the electron motion. The vector potential determines the change in phase of the wave function which, unlike in classical physics, can not be arbitrary but rather is restricted

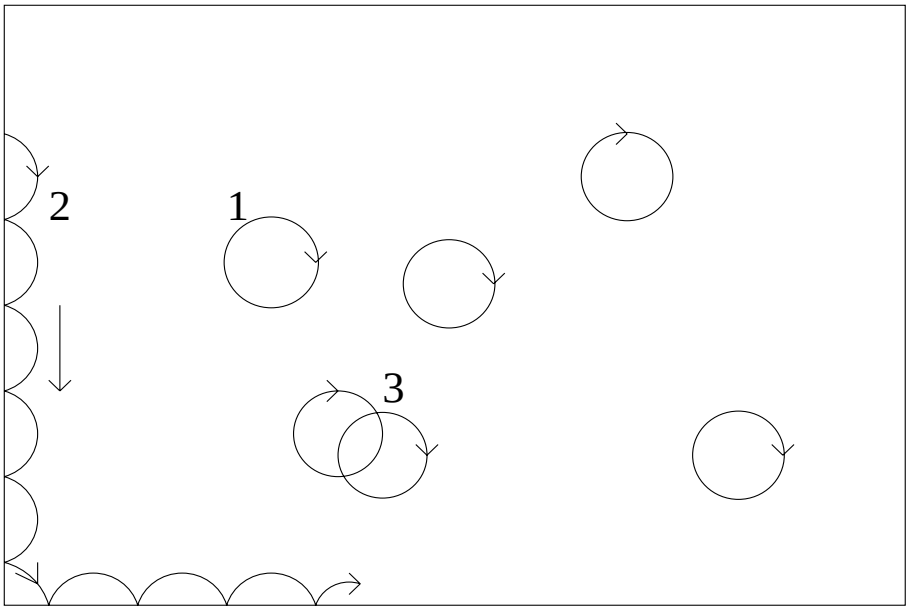

Figure 1. Electron orbits in a magnetic field. 1 - bulk electrons; 2 - surface electrons; 3 - electron orbit perturbed by scattering. Vertical arrow shows direction of rotation of surface electrons opposite to the sense of rotation of bulk electrons.

by the requirement of phase quantization which follows from the requirement of singe-valuedness of the wave function. The wave function becomes "rigid", to a certain extent, in a way similar to London's treatment of the rigidness of the wave function in a superconductor.

Current density in a metal is given by an expression

$$\mathbf{j} = \frac{Ne}{m}(\mathbf{p} - \frac{e}{c}\mathbf{A}) \tag{2}$$

where the first term related to momentum $\mathbf{p}$ is called "paramagnetic current" whereas the second one is the "diamagnetic current". In classical physics, both current components cancel each other, in compliance with the van Leeuwen theorem, but quantum mechanically paramagnetic current

$$\mathbf{j}_p = \frac{ie\hbar}{2m}(\psi\nabla\psi^* - \psi^*\nabla\psi) \tag{3}$$

attains only discreet values since the wave function in the ring

$$\psi = \frac{1}{\sqrt{L}}e^{in\theta}, \quad n = 0, \pm1, \pm2, ... \tag{4}$$

has a quantized value of the phase $n\theta$ (θ is the azimuthal angle in a ring). Thus, the cancellation between $\mathbf{j}_p$ and $\mathbf{j}_d$ is only possible at discrete values of magnetic flux $\Phi = n \cdot hc/e$. Therefore the current is a periodic function of flux with a period

$$\Phi_0 = \frac{hc}{e}. \tag{5}$$

The above explanation of persistent (or "permanent", or "non-decaying") current is similar to London interpretation of persistence of current in a superconductor arguing that it is a result of "rigidness" of its wave function such that it remains same at finite vector potential $\mathbf{A}$ as it is at $\mathbf{A} = 0$ when there is no current,

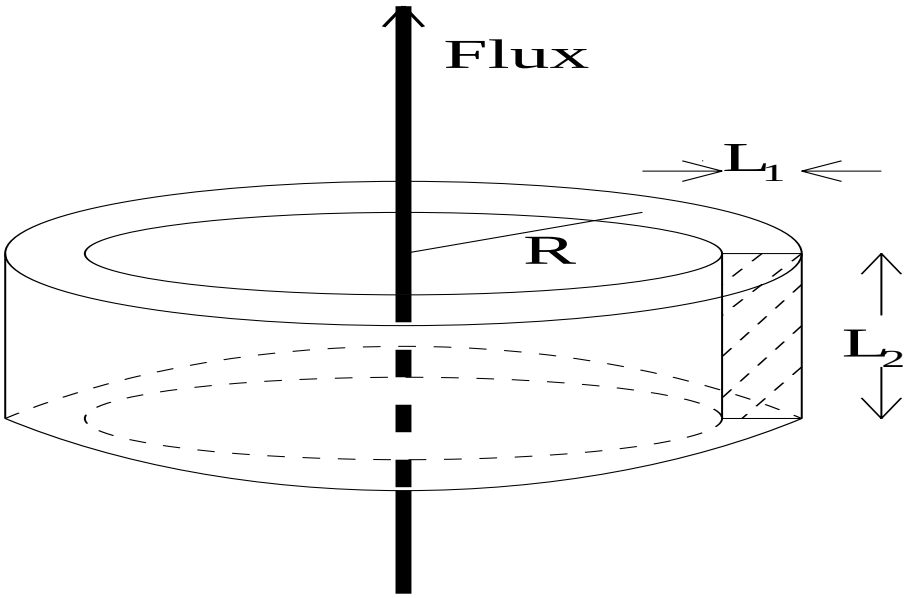

Figure 2. Aharonov-Bohm loop of radius R, cross sectional area $S_0 = L_1 L_2$, and the source of magnetic flux in form of thin solenoid piercing the ring.

but the current appears at $\mathbf{A} \neq 0$ since paramagnetic current remains frozen to zero. The microscopic theory of superconductivity proves that the rigidness of the wave function is the consequence of the existence of the energy gap Δ[15], and that the flux quantum in a superconductor

$$\Phi_s = \frac{hc}{2e} \tag{6}$$

is twice smaller than Φ_0 due to electron pairing.

The rigidness of the wave function in normal metal is insured by an effective gap in the excitation spectrum of electrons equal to the distance between the quantized eigenstates at Fermi energy

$$\Delta\varepsilon = \frac{hv_F}{L} \tag{7}$$

where v_F is the Fermi momentum of electron and $L = 2\pi R$ is the circumference of the ring. Observation of persistent current requires low temperature $T \ll \Delta\varepsilon$ and is therefore the "mesoscopic" effect existing at small L (typically, $L < 1\mu m$) and corresponds to the value of persistent current of the order

$$J_{\max} \simeq J_0 \eta_1(T)\eta_2(N_e) \tag{8}$$

where

$$J_0 = \frac{ev_F}{L} \tag{9}$$

and

$$\eta_1 \simeq \exp(-2\pi^2 \Delta\varepsilon/T) \tag{10}$$

is a temperature factor[2]. η_2 is the geometric factor taking into consideration the contribution of all electrons with the quantized energies

$$\varepsilon_{nn_1n_2} = \frac{h^2}{2mL^2}(n - \frac{\Phi}{\Phi_0})^2 + \frac{h^2}{2mL_1^2}n_1^2 + \frac{h^2}{2mL_2^2}n_2^2 \tag{11}$$

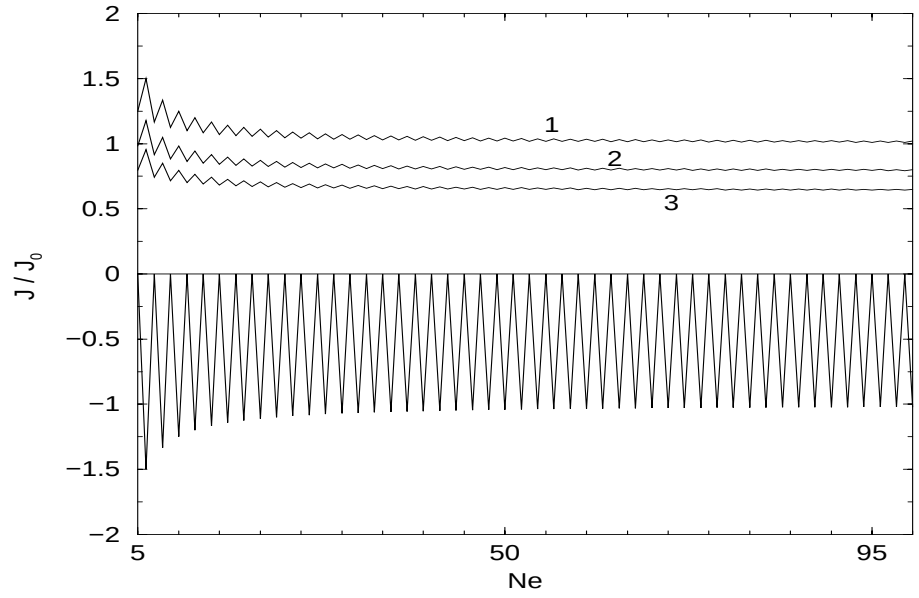

Figure 3. Persistent current as a function of number of electrons N_e in the $1d$ ring. 1 - maximal value of $J(\Phi)$ normalized to $J_0 = ev_F/L$, at given N_e; 2 - amplitude of first harmonic $J^{(1)}/J_0$; 3 - maximal current estimated as ratio of $\Delta E(\Phi)$ between $\Phi = -\Phi_0/2$ and $\Phi = \Phi_0/2$ to Φ_0. Lower curve shows spontaneous persistent current (see below).

including the states along the ring (quantum number $n = 0, \pm 1, ...$) and the discrete states in the perpendicular direction ($n_{1,2} = 1, 2, ...$). The value of η_2 is larger than 1 due to large number of perpendicular channels (typically, $J_{\max} \geq 10 - 100\ nA$ at $L < 1\mu$m). Some estimates give $\eta_2 \sim N_\perp^{1/2}$ where $N_\perp$ is the number of perpendicular channels (the number of states with quantized perpendicular momenta at Fermi energy, $N_\perp = k_F^2 S_0/2\pi^2$; S_0 is the cross section of the ring, see Fig.2).

Fig.3 shows dependence of maximal persistent current on the number of electrons in $1d$ ring ($N_\perp = 1$), and Fig.4 in the $3d$ ring with a finite cross section S_0 (We assume the fixed-N_e sample.) In the latter case, the dependence is not regular and not periodic. The states (11) with corresponding flux shifts add to total current in an almost chaotic way such that only few last (largest energy) contributions make the main effect. Nevertheless, other states also contribute making drift of $J_{\max}$ up, i.e. to higher than ev_F/L values. At large N_e, the dependence $J(\Phi)$ at fixed N_e is nonsinusoidal (see Fig.5) and can be presented as sum of harmonics

$$J(\Phi) = \sum_{m=1}^{\infty} J^{(m)} \sin 2\pi \frac{m\Phi}{\Phi_0} \tag{12}$$

corresponding to "flux quanta" with multiple charges $e, 2e, 3e, ...$

Persistent current is a voltage-free non-decaying current which exists as a manifestation of the fact that the ground state of a double connected conductor in a magnetic field is a current-carrying one. This statement was proved for the ballistic loops [2] as well as for the diffusive rings [4]. There is no principal difference between these two extremes. Ballistic mesoscopic structure doesn't show infinite conductivity at a finite *d.c.* voltage, and a *d.c.* resistance of the loop is infinite rather than zero when an electric field is applied to system. In case when the *current* is fed through the structure, no voltage appears provided the magnitude of the current is smaller than the critical value. This applies to both elastic and inelastic scatterings. The magnitude of critical current in the ballistic ring smoothly matches the current of the

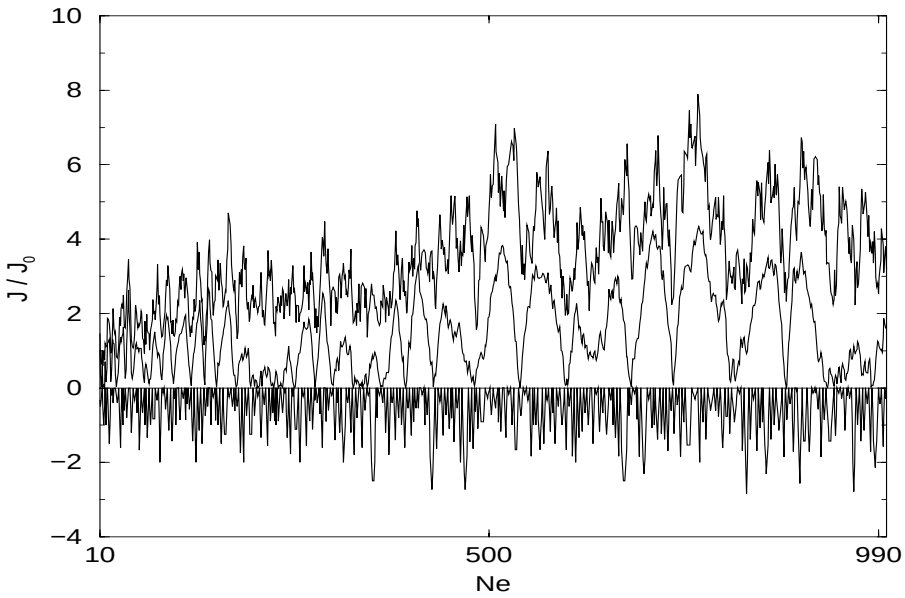

Figure 4. Persistent current as a function of number of electrons in the ring with the circumference to cross-sectional dimensions ratio $L : L_1 : L_2 = 10 : 3 : 3$. Upper curve - maximal current in units of J_0 corresponding to given N_e; middle curve - amplitude of normalized first harmonics; lower curve - spontaneous persistent current, also in units of J_0. These dependences are illustrative, for simplicity we consider the case of "spinless" electrons.

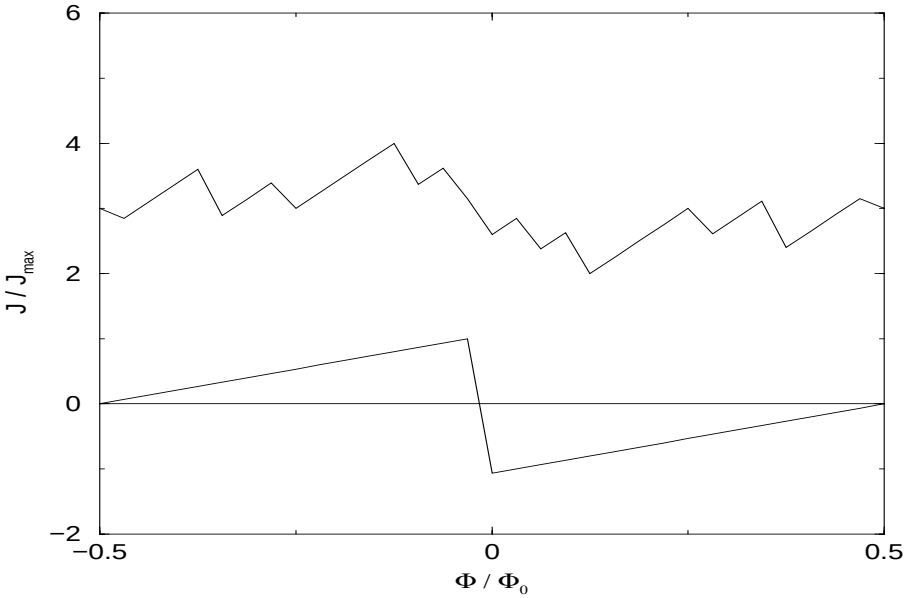

Figure 5. Illustrative examples of persistent current versus Aharonov-Bohm flux dependences taken at $N_e = 100$. Lower curve corresponds to $1d$ ring, the upper curve (shifted for convenience up and normalized, as well as the upper one, to maximal current at given N_e and L) in a ring with $L : L_1 : L_2 = 10 : 3 : 3$.

diffusive ring when the mean free path becomes large. In a dirty limit, $l \ll L$, where l is the elastic mean free path of electron, critical value of persistent current decreases proportional to l/L according to Ref [16], or to $(l/L)^{1/2}$ according to numeric simulation [14]. The persistent current doesn't even require severe restriction on the so called "phase breaking" mean free path l_φ. In fact, the normal-metal supercurrent is an analogue of the "incoherent" Josephson current [17, 18], the one in which the phase of the pair wavefunction in superconductor is considered as a classical variable. Stronger criteria (the dephasing length larger than the system size, and the analogous requirement in the time domain, that the "decoherence time" is larger than the characteristic time of observation) apply to persistent current rings as quantum computational tools mentioned above, which are the analogues of the macroscopic quantum tunneling [19, 20, 21].

Observation of persistent currents have been done in an indirect [22,23] as well as in the direct [5, 6, 7] experiments showing the single-flux-quantum periodicity in the resistance, and in the first harmonic nonlinear output, in thin Nb wires [22], networks of isolated Cu rings [23], and in stand-alone metallic [5], semiconducting [6] and macromolecular [7] Aharonov-Bohm loops. The last experiment was actually interpreted by authors in terms of the antiferromagnetic ordering regardless their own mentioning of the *nonmagnetic* character of given macromolecule (a "ferric wheel" $[Fe(OMe)_2(O_2CCH_2Cl)]_{10}$). In recent publications [8, 24, 25], macromolecular and nanoscopic Aharonov-Bohm structures have been suggested as elements of quantum computers.

3. Spontaneous persistent currents

In special symmetric configuration, mesoscopic loop can support persistent current even when Aharonov-Bohm flux is *not* applied to system [9]. This accomplishes as a bistable state such that infinitely small nonzero flux triggers the loop into one of its two equal-energy opposite-direction persistent current configurations. On the other hand, the lattice (the atomic configuration of the loop) can respond to such a degenerate ground state by making the atom readjustment similar to Peierls transition (doubling of the lattice period in one-dimensional atomic chain). In fact, such possibility clearly shows up in the case of $1d$ loop with the discrete quantum states (11) at $n_1 = n_2 = 0$ corresponding to energies

$$\varepsilon_n = \frac{\hbar^2}{2mR^2}(n - f)^2 \tag{13}$$

where $n = 0, \pm 1, \pm 2, ...$ and $f = \Phi/\Phi_0$ is magnetic flux threading the loop in units of flux quantum $\Phi_0 = 4 \cdot 10^{-7} Gs \cdot cm^2$. In Figs.3,4, we showed persistent current in $1d$ and $3d$ rings as function of electron population. The current vanishes when all states $\pm$ at given electron number N_e are equally populated at $f = 0$.

As an example, the loop with 3 electrons has energies

$$E(f) = \varepsilon_0[f^2 + \frac{1}{2}(\pm 1 - f)^2] + \frac{LJ_0^2}{2c^2} j^2(f) \tag{14}$$

corresponding to two spin-1/2 states with $n = 0$, and one state with $n = 1$ or $n = -1$. The last term in Eq.(14) is the magnetic inductive energy and L is an inductance (of the order of the ring circumference, in the units adopted). The current

$$J = -\frac{e}{h}\partial E/\partial f \tag{15}$$

equals to

$$J(f) = J_0(\pm 1 - 3|f|), \quad J_0 = e\varepsilon_0/h \tag{16}$$

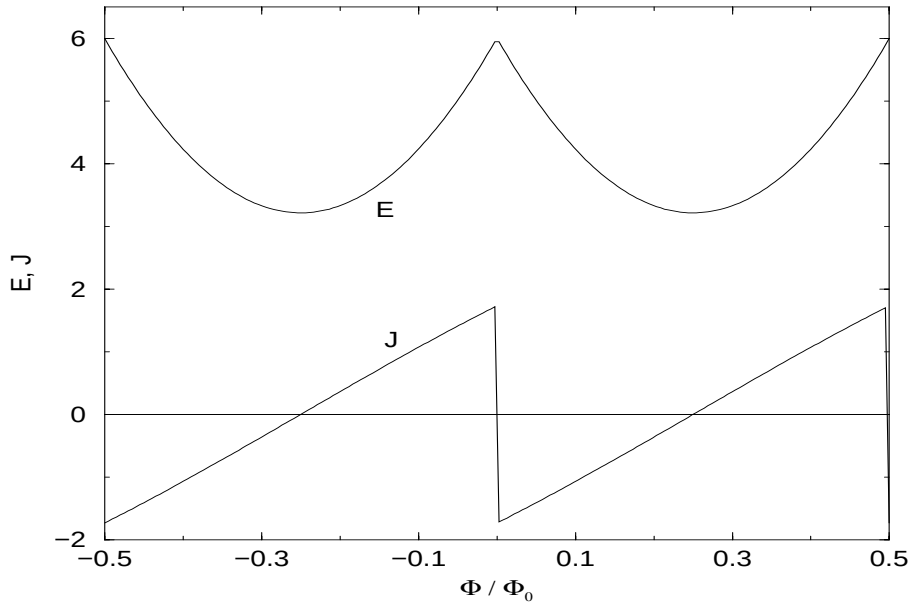

Figure 6. Lower curve: Current versus magnetic flux in the 3-site loop with 3 noninteracting electrons. Upper curve: Energy vs flux for $N = 3, n = 3$ loop at the value of hopping parameter $t_0 = -1$. Energy is rescaled and arbitrarily shifted up for clarity.

and is nonzero at $f = 0$ in either of states "+" or "−", see Fig.6. The ratio of magnetic energy to kinetic energy is of the order

$$\eta = \frac{LJ_0^2}{2c^2\varepsilon_0} \simeq \frac{e^2}{4\pi mc^2 R} \sim 10^{-6}\frac{a_0}{R} \tag{17}$$

where a_0 is the Bohr radius. This is a very small quantity, and therefore the magnetic energy is unimportant in the energy balance of the loop. The flux in the loop $f = f_{ext} + 2\eta j(f)$ where f_{ext} is an external flux and $j(f) = J(f)/J_0$. Correction to externally applied flux is only essential at $f_{ext} \sim \eta$ otherwise we can ignore this contribution.

The property of nonzero persistent current thus demonstrated for the noninteracting electrons, survives strong electron-electron coupling but collapses when the coupling to the lattice is included (see below). Nevertheless, when the loop is on the rigid background (say, cyclic molecule on a substrate of much harder bound solid) the degeneracy may be not lifted, or may remain in a very narrow interval of externally applied fields. We will investigate this possibility in the tight binding approximation [14], in which electrons are tightly bound to certain atomic locations (traps), and make the loop conducting by resonant tunneling between these locations.

In the tight binding approximation, Hamiltonian of the loop in the second quantized form reads

$$H = \sum_{i=1}^{N}(t_j a^+_{j\sigma}a_{j+1,\sigma}e^{i\alpha_j} + \text{h.c.} + U\sum_{i=1}^{N} n_{i\uparrow}n_{i\downarrow} + V\sum_{i=1,\sigma,\sigma'}^{N} n_{i\sigma}n_{i+1,\sigma'} + \frac{1}{2}K\sum_{j=1}^{N}(\theta_j - \theta_{j+1})^2 \tag{18}$$

where t_j is the hopping amplitude between two near configurational sites, j and $j+1$,

$$t_j = t_0 + g(\theta_j - \theta_{j+1}) \tag{19}$$

and

$$n_{i\sigma} = a^+_{i\sigma}a_{i\sigma} \tag{20}$$

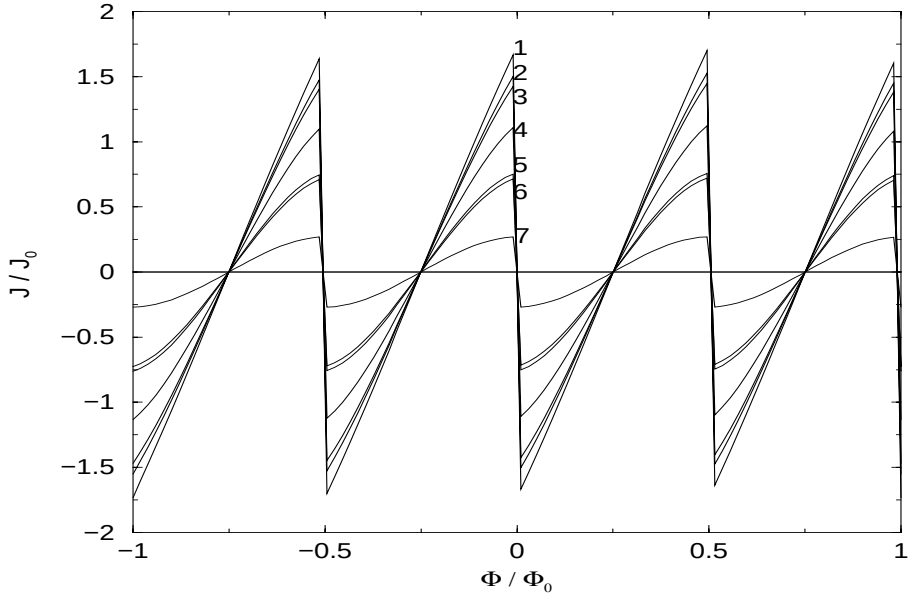

Figure 7. Spontaneous persistent current versus flux for $t_0 = -1$ and various values of Hubbard parameter U: 1 - $U = 0$; 2 - $U = -2$; 3 - $U = 2$; 4 - $U = -5$; 5 - $U = 5$; 6 - $U = -10$; 7 - $U = 10$.

is the number operator. α_j is the Aharonov-Bohm phase (a Peierls substitution for the phase of hopping amplitude)

$$\alpha_j = \frac{2\pi f}{N} + (\theta_j - \theta_{j+1})f. \tag{21}$$

$a^+_{j\sigma}$ is the creation (and $a_{j\sigma}$, the annihilation) operator of electron at site j with spin σ. θ_j with $j = 1, 2, ..., N$ are the angles of distortion of site locations from their equilibrium positions $\theta^0_j = 2\pi j/N$ satisfying the requirement $\sum_{j=1}^{N} \theta^0_j = 0$, and g is the electron-phonon coupling constant. The interaction (19) reflects the property that the hopping amplitude depends on the distance between the localization positions and assumes that the displacement $\theta_j - \theta_{j+1}$ is small in comparison to $2\pi/N$. U and V are Hubbard parameters of the on-site and intra-site interactions. The parameters are assumed such that system is not superconductive (e.g., $U > 0$; and anyway, the superconductivity is not allowed for $1d$ system; it is ruled out for small system). The last term in Hamiltonian (18) is the elastic energy and K is the stiffness parameter of the lattice.

In the smallest loop, the one with three sites ($N = 3$), only two free parameters of the lattice displacement, X_1 and X_2, remain

$$\theta_1 = X_1 + X_2, \quad \theta_2 = -X_1 + X_2, \quad \theta_3 = -2X_2 \tag{22}$$

which are decomposed to second-quantized Bose operators b_1, b_2 as

$$X_1 = (\frac{3K}{\omega})^{1/4}(b_1 + b_1^+), \quad X_2 = 3(\frac{K}{3\omega})^{1/4}(b_2 + b_2^+). \tag{23}$$

The system (18) is solved numerically with the ABC compiler [26] which includes the creation-annihilation operators as its parameter types. These are generated as compiler macros with sparse matrices

$$A_n = (u\otimes)^{N_1+N_2-n} a (\otimes v)^{n-1} \tag{24}$$

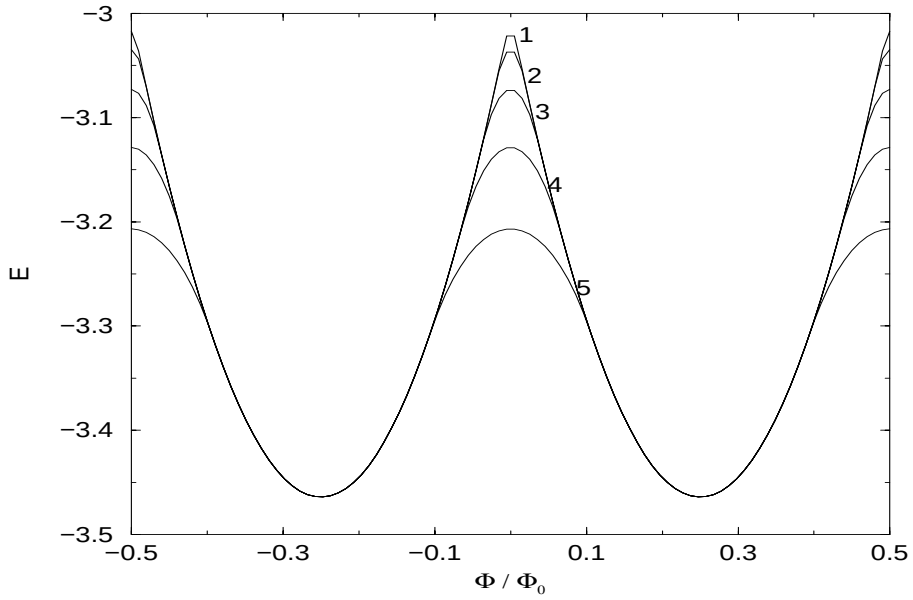

Figure 8. Energy vs flux in a loop with noninteracting electrons coupled to lattice with the value of coupling parameter $g = 1$ and various values of the stiffness parameter K: 1 - K=2; 2 - K=3; 3 - K=5; 4 - K=10; 5 - K=20.

where a, u, v are 2×2 matrices ($\otimes$ is the symbol of Kronecker matrix product)

$$a = \begin{pmatrix} 0 & 0 \\ 1 & 0 \end{pmatrix}, \quad u = \begin{pmatrix} 1 & 0 \\ 0 & 1 \end{pmatrix}, \quad v = \begin{pmatrix} 1 & 0 \\ 0 & \eta \end{pmatrix} \tag{25}$$

and η is a parameter

$$\eta = \begin{cases} -1, & \text{at} \quad n = 1, 2, ..., N_1 & \text{Fermionic sector} \\ 1, & \text{at} \quad n = N_1 + 1, ..., N_1 + N_2 & \text{Bosonic sector} \end{cases} \tag{26}$$

Bosons are considered as "hard-core bosons" such that there are only two discrete states for each mode of displacement. We calculate the ground state of Hamiltonian (18) as function of magnetic flux f (a classical variable). In application to real atomic (macromolecular) systems, we can consider X_1, X_2 as classical variables since quantum uncertainties in the coordinates ($\Delta X_{1,2} \sim (\hbar/M\omega)^{1/2}$) are typically much smaller than the interatomic distances (M is the mass of atom and $\omega \sim 10^{13} s^{-1}$ is the characteristic vibration frequency). The energy of the loop is calculated as function of X_1, X_2 and further minimized with respect to X_1, X_2 for each value of f. The nonzero values of X_1, X_2 will signify the "lattice" (the ionic core of the macromolecule) instability against the structural transformation which is analogous to Peierls transition.

In the noninteracting system ($U, V, g = 0$), the energy versus flux f shows kink with a maximum at $f = 0$ (Fig. 6) in the half filling case, i.e. at the number of electrons n equal to the number of sites, N, as well as in a broader range of near the half-filling values of n at larger N. Actually, such dependence is typical for any $N \geq 3$ system for a number of (fixed) values of n.

The 3-site loop $E(f)$ dependence is shown in Fig.6 together with the dependence of the current on f. The latter shows discontinuity of current $J(f)$ at $f = 0$ of the same order of magnitude as the standard value of persistent current. The current at $f = 0$ is *paramagnetic* since energy vs flux has *maximum* rather than minimum at $f = 0$. On-site interaction reduces the amplitude of persistent current near zero flux (Fig.7) but doesn't remove its discontinuity at $f = 0$. Therefore, the most strong opponent of the Aharonov-Bohm effect, the electron-electron interaction, leaves it practically unchanged.

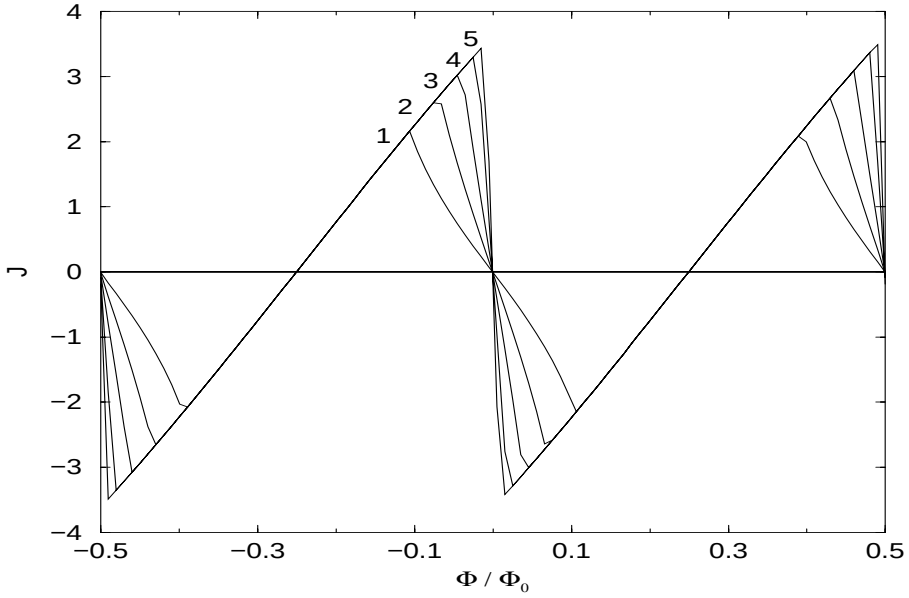

Figure 9. Energy vs flux for a loop with coupling constant $g = 1$ and various values of stiffness K: 1 - K=2; 2 - K=3; 3 - K=5; 4 - K=10; 5 - K=20.

On the other hand, the electron-phonon interaction flattens the $E(f)$ dependence near the peak value, see Fig.8. At large stiffnesses, K, this flattening remains important only for small magnetic fluxes, much smaller than the flux quantization period $\Delta\Phi = \Phi_0$. Mention that persistent current peak reduces in its amplitude only slightly near the zero flux. As is seen from Fig.9, electron-phonon interaction splits the singularity at $\Phi = 0$ to two singularities at $\Phi = \pm\Phi_{sing}$. Outside the interval $-\Phi_{sing} < \Phi < \Phi_{sing}$, Peierls transformation is blocked by the Aharonov-Bohm flux. The range of magnetic fluxes between $-\Phi_{sing}$ and Φ_{sing} determines the domain of the developing lattice transformation which signifies itself with the nonzero values of lattice deformation X_1, X_2. The latter property allows us to suggest that the spontaneous persistent current state (a peak of dissipationless charge transport at, or near, the zero flux) remains at the nonzero flux when the electron-phonon coupling is not too strong or when the lattice stiffness is larger than certain critical value.

4. Aharonov-Bohm qubits and qugates

Quantum computation [27] is a promising field for solving intractable mathematical problems, those in which the number of computational steps (if solved with a classical computer) increases exponentially with the number of computational units (M), e.g., number of spins in the Heisenberg ferromagnet, number of electrons and lattice sites in the Hubbard model of solid, number of binary digits in a large integer to be factorized, etc. If these units (spins, atoms, digits) are represented as "quantum bits" and processed by unitary transformations acted upon by the logical quantum gates, at least some of these problems can be solved in a polynomial time in M (e.g., the Shor's algorithm [28] for factorizing large integers). Basically, the fundamental gates are unitary time evolutions for given Hamiltonians executed on qubits or on pairs of qubits and for certain time intervals. Fundamental gates are known to be the unitary operations such as the single qubit bit-flip, phase-flip and the Hadamard transformations and the double qubit controlled-NOT (CNOT) operation [27]. Workers in the field at earlier times considered qubit realizations as quantum optical or atomic systems, and shifted at more recent times to other methods employing mesoscopic condensed matter structures (quantum dots [29], superconducting Cooper-pair boxes [30, 31, 32, 33], flux-state Josephson

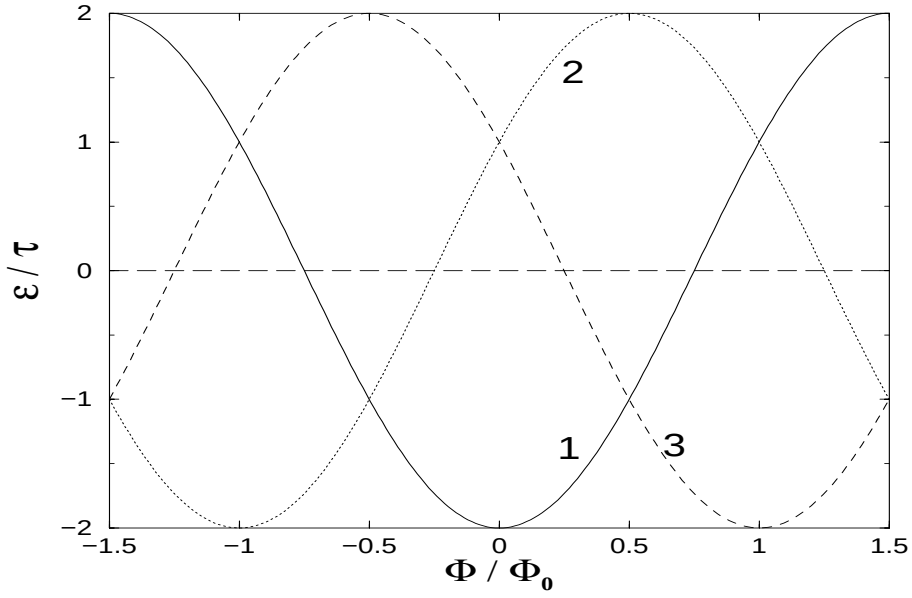

Figure 10. Operational diagram of the Aharonov-Bohm qubit. Curves 1 and 3 are energy versus magnetic flux dependences in the degenerate states carrying opposite currents $\pm j = -c\partial\varepsilon/\partial\Phi$ (full and dashed lines). Curve 2 corresponds to the zero-current virtual state at the operating point of qubit at half-flux quantum $\Phi = \Phi_0/2$ (a control state, the dotted line). This state couples qubit to the logical qugate.

junctions [34, 35, 36]). In Ref.[37], the necessary conditions for quantum computation have been specified, not all of which have already achieved perfect realization (the problems with the solid-state qubits are documented in Refs. [38, 39]). This leaves space for more suggestions of the instrumental realization of qubits, especially those that use the solid state technology. We investigated this new possibility[8] employing the three state quantum logic with doubly degenerate qubit states accompanied by a third (auxiliary) level based on 3-site Aharonov-Bohm loop.

The auxiliary level is used to coherently couple the operational qubit states to the computational environment including the other qubits as well as the input-output devices. The proposed structure is naturally realized with the quantum states of the ring of metallic islands (or atomic sites) connected by resonant tunnelling in the presence of the Aharonov-Bohm flux threading the ring, a persistent-current, and placed in an external electric field perpendicular to the magnetic flux to perform the qugate manipulation in the invariant subspace of two degenerate states. We focus in this work on the quantum mechanical aspects of qubit and qugate operations with persistent current (PC) loops.

In the mesoscopic ring of a normal metal of size L, smaller than the phase-decoherence length of the electrons, the charge current is produced under the influence of the Aharonov-Bohm flux. Physically, the shifted energy minimum in the presence of the Aharonov-Bohm flux is counterbalanced by a net charge flow producing a persistent current in the absence of resistive effects. The magnitude of the persistent current in a clean metallic ring of circumference L is typically given by Eq. (7). In a nanoscopic (atomically small) ring with discrete sites and with one electron, the magnitude of the persistent current is

$$J_{\max} = \frac{2e\tau}{N\hbar} \sin\frac{\pi}{N} \simeq 2\pi e\tau/\hbar N^2 \tag{27}$$

where N is the number of sites in the discrete ring and τ is the electron hopping amplitude between the sites. The PC is created individually by single electrons hence the fundamental flux quantum $\Phi_0 = hc/e$ is twice larger than the Abrikosov or Josephson flux quantum $\Phi_s = hc/2e$. This very fact may permit new

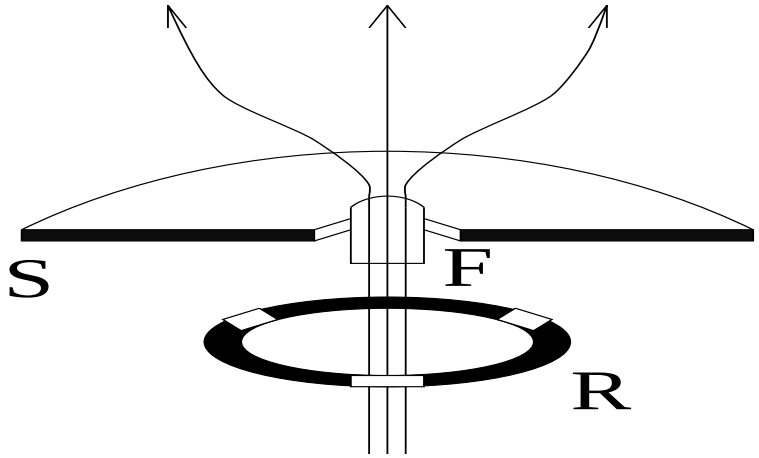

Figure 11. A sketch of the magnetically focused lines of the magnetic field from the superconducting fluxon trapped in the opening of superconducting foil (S), compressed by ferromagnetic crystal (F) and directed into the interior of PC ring (R).

effects to arise when a single Josephson vortex or Abrikosov fluxon is used to manipulate the single electron current in the PC ring.

The Hamiltonian of the system is

$$H = -\tau \sum_{n=0}^{N-1} (a_n^+ a_{n+1} e^{i\alpha} + a_{n+1}^+ a_n e^{-i\alpha}) \tag{28}$$

where a_n^+ is a fermionic operator creating (and a_n, annihilating) electron at site $\mathbf{R}_n$ in a ring with the periodic boundary condition $a_N = a_0$, and α is the phase related to the Aharonov-Bohm flux threading the ring by $\alpha = 2\pi\Phi/N\Phi_0$. The Hamiltonian (28) is diagonalized by the angular momentum (i.e., $m = 0, 1, \ldots, N-1$) eigenstates $A_m^+|0\rangle$

$$A_m^+ = \frac{1}{\sqrt{N}} \sum_{n=0}^{N-1} e^{2\pi i m n/N} a_n^+ \tag{29}$$

with the site energies

$$\varepsilon_m = -2\tau \cos \frac{2\pi}{N}(m - \frac{\Phi}{\Phi_0}) \tag{30}$$

plotted against the normalized flux Φ/Φ_0 in Fig.10.

Since two ground states are degenerate at $\Phi_0/2$, they can be used as the components of the qubit while the third one couples the qubit to a qugate, to be discussed below. One possible practical realization of the qubit with an appropriate architecture is sketched in Fig.11. The horizontal ring (R) may be realized as a three-sectional normal-metal intersected by insulating tunnelling barriers (or consisting of overlapping metallic films separated by thin oxide layers). Creating strong magnetic field to operate the qubit at the half quantum flux is suggested with the help of superconducting fluxon trapped in a hole inside the superconducting film, with the magnetic field lines further focused by a mesoscopic ferromagnetic cylinder near the ring.

The isolated qubit structure can in principle be realized as a three-site defect in an insulating crystal, similar to the negative-ion triple vacancies (known as F_3-centers) in the alkali halide crystals (e.g., see [40]).

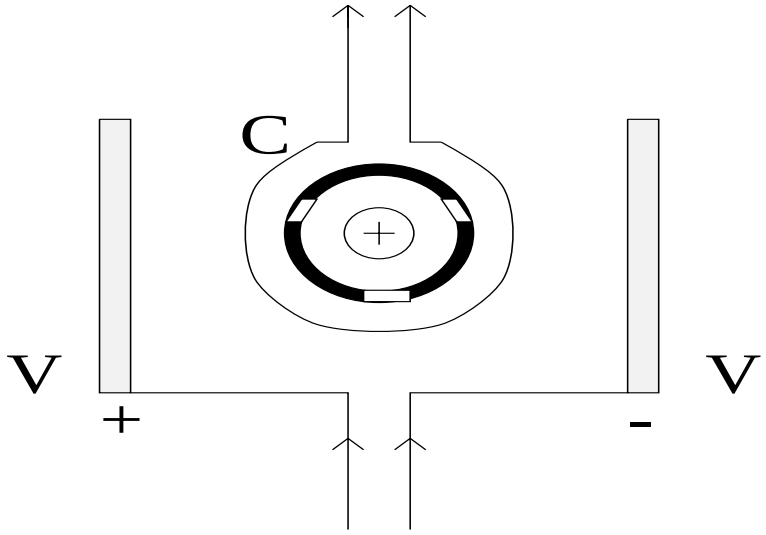

Figure 12. A sketch of the bit flip. Loop C is an output coil, V's are the electrodes creating electric field perpendicular to the magnetic field (normal to sheet) in a qubit.

Yet another possibility may be to use the natural molecular conductors, the carbon nanotubes [41], with a proper configuration of carbon atoms in a helical tube, or the nanotubes covered by metallic nanolayers [42]. In such a structure, the single qubit related gate manipulations are provided by applying an electric field perpendicular to the Aharonov-Bohm flux. It will be shown below that, facilitated by the auxiliary level as well as the crossed electric and Aharonob-Bohm fields, all fundamental qugate operations can be performed in the qubit subspace.

In the eigen basis of the operators A_m (the angular momentum basis), the Hamiltonian (28) in the absence of the electric field is transformed into the diagonal form (we scale all energies in units of τ)

$$H_0 = \sum_m \varepsilon_m A_m^+ A_m = \begin{pmatrix} -1 & 0 & 0 \\ 0 & 2 & 0 \\ 0 & 0 & -1 \end{pmatrix}. \tag{31}$$

Once the static electric field is on the generated electrostatic potential between the metallic islands is given by $V_n = V_0 \cos(2\pi n/3)$ where for $n = 0$, V_0 is the reference potential referring to the zeroth island. The electrostatic potential, as depicted in Fig.12, is represented in the angular momentum basis by the constant nondiagonal symmetric matrix

$$H_1(V_0) = \begin{pmatrix} 0 & v & v \\ v & 0 & v \\ v & v & 0 \end{pmatrix} \tag{32}$$

where $v = V_0/2\tau$. For the manifestation of the single qubit qugates, two more interaction terms are defined.

The first one is the static *site potential* V_S represented by the Hamiltonian H_2

$$H_2 = v_s \mathrm{diag}(1, 1, 1) \tag{33}$$

where $v_s = V_s/\tau$. The second term receives by shifting magnetic flux away from $\Phi_0/2$. It is described by the diagonal Hamiltonian H_3

$$H_3 = \mathrm{diag}(\Delta\varepsilon_1, \Delta\varepsilon_2, \Delta\varepsilon_3) \tag{34}$$

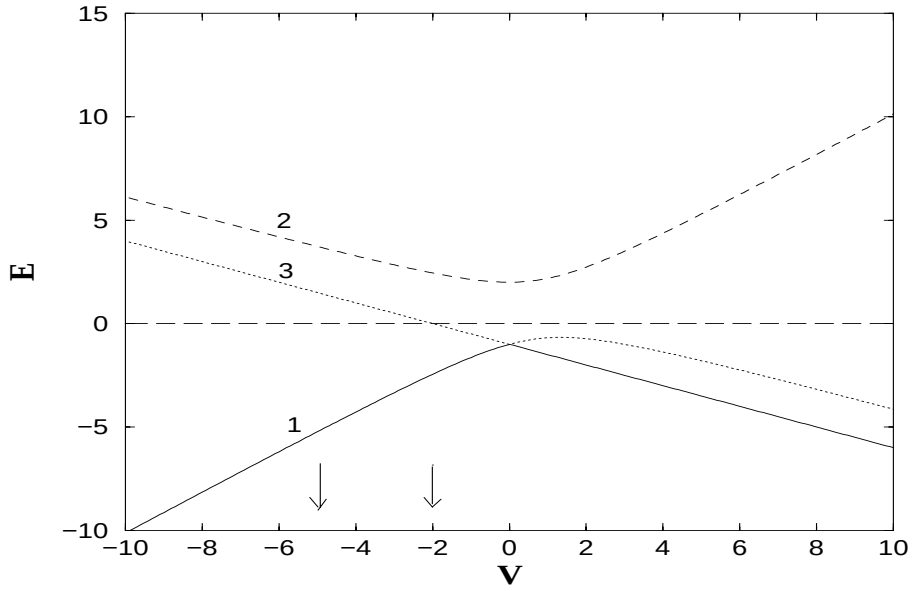

Figure 13. Energy versus electrostatic potential. 1 and 3 (solid line and dotted line) are the energies which become degenerate at $V_0 = 0$, and 2 (the dashed line) is an energy of the auxiliary control state $|c\rangle$. The arrows indicate the values of the potential V_0 corresponding to the operational points of the bit-flip (i.e. G_1) and G_3 (i.e. Hadamard) gates.

where Δ_i's are shifts in energy corresponding to non-half integer flux. It is shown below that the first two Hamiltonians H_0 and H_1 are sufficient in the realization of the fundamental single qubit gates except the phase shift. On the other hand, the Hamiltonians H_2 and H_3 generate relative phase shifts between the qubit states. If one denotes an arbitrary superposition state in the angular momentum basis, the time dependence of the amplitudes $C_n(t)$ are given by

$$C_n(t) = \sum_m [\exp(-iHt)]_{mn} C_m(0) \tag{35}$$

in which, in general, $H = (H_0 + H_1 + H_2 + H_3)$. Different terms in the total Hamiltonian H are controlled by the time dependent ideal step function switches.

Let us first consider the case $V_S = 0$ and $\Phi = \Phi_0/2$ when both H_2 and H_3 are switched off. When the interaction H_1 is turned on by a step function switch for a time t, the amplitudes are found by

$$C_n(t) = \sum_{m,k} S^{-1}_{kn}(V_0) e^{-iE_k t} S_{mk}(V_0) C_m(0) \tag{36}$$

where $E_k(V_0)$ are the eigenenergies of Hamiltonian $H_0 + H_1(V_0)$ and $S_{nm}(V_0)$ are the unitary matrices transforming from the noninteracting eigenbasis (the one corresponding to H_0) to the eigenbasis of the full Hamiltonian $H_0 + H_1$. It is indicated by Eq.(36) that, at fixed V_0, the time evolution of the states is performed by the interplay of the three different eigenenergies. This is sufficient evidence that if the eigenenergies are appropriately adjusted the population of the auxiliary state (in the angular momentum basis) can be made to vanish under certain initial conditions. At these moments, the three state system instantaneously collapses onto the qubit subspace without loss of any information if the auxiliary state was unoccupied initially. Furthermore, we also require the Hamiltonian to have performed the given qugate in the qubit subspace. A necessary condition for the instantaneous collapse onto the qubit subspace is a commensuration condition between the eigenenergies $E_k(V_0)$, $(k = 1, 2, 3)$ so that exponential factors in Eq.

(37) destructively interfere at fixed time instants to destroy the nondiagonal correlations. The eigenenergies $E_k(V)$ are plotted in Fig.13. The required commensuration condition can be manifested by

$$E_3 - E_1 = K\,(E_2 - E_3) \tag{37}$$

for integer K. Eq. (36) guarantees the periodic collapses of the wavefunction onto the desired basis and the next step is to search whether the desired qugate operations could be realized simultaneously in this desired basis. Since the integer K is at our disposal, it can be changed numerically to search for the desired qugate operations. For the corresponding values of the potential respecting Eq.(37) we find

$$V_0(K) = -\frac{2}{3K}[K^2 + K + 1 + (K-1)\sqrt{K^2 + 4K + 1}]. \tag{38}$$

In particular we mention that for $K = 1$ one has $V_0^{(1)} = -2$; and at $K = 3$ one has $V_0^{(3)} = -\frac{2}{9}(13 + 2\sqrt{22}) = -4.9735$ and we succeeded in finding two qugates in our first few attempts. As shown below, these two cases yield the bit-flip and Hadamard transformations. The $K = 1$ case can be explicitly proved by checking the identity

$$\exp\{-it\begin{pmatrix}-1 & -1 & -1\\ -1 & 2 & -1\\ -1 & -1 & -1\end{pmatrix}\} = \frac{1}{2}\begin{pmatrix}1+c+s & s & -1+c+s\\ s & 2(c-s) & s\\ -1+c+s & s & 1+c+s\end{pmatrix} \tag{39}$$

where it is defined that $c = \cos(t\sqrt{6})$, $s = i\sqrt{\frac{2}{3}}\sin(t\sqrt{6})$. At $s = 0$ (i.e. $c = \pm 1$), the transformation matrix of Eq.(39) block-diagonalizes in a subspace of states 1,3 (i.e. $|0\rangle$, $|1\rangle$, the qubit states) and the upper state 2 (i.e. $|c\rangle$, the auxiliary "control" state). In particular, for $c = -1$ the bit-flip is performed between the qubit states.

In Figs.14,15 the populations of the states $p_n(t) = |C_n(t)|^2$ are plotted for the mentioned cases $K = 1$ and $K = 3$. The instantaneous collapse onto the qubit subspace is obtained at $t = t_1$ for $K = 1$, and at $t = t_3$ for $K = 3$, if the auxiliary level is unoccupied at $t = 0$. We found these critical times as (in units of $\hbar/\tau$)

$$t_1 = \frac{\pi}{\sqrt{6}} = 1.2825, \quad t_3 = \frac{\pi}{2[E_2(V_0) - E_3(V_0)]_{K=3}} = 0.7043 \tag{40}$$

where the eigenenergies are

$$E_{1,3}(V_0) = \frac{1 + V_0/2}{2} \mp \frac{3}{2}\sqrt{1 - V_0/2 + V_0^2/4}, \quad E_2(V_0) = -1 - V_0/2 \tag{41}$$

for $V_0 \le 0$. We notice that the configuration $(t_1, K = 1)$ performs the bit-flip $|0\rangle \leftrightarrow |1\rangle$ whereas $(t_3, K = 3)$ creates the equally populated Hadamard-like superpositions of $|0\rangle$ and $|1\rangle$. These operations are presented in the qubit subspace by the matrices (overall phases are not shown)

$$G_1 = \begin{pmatrix}0 & 1\\ 1 & 0\end{pmatrix} \text{ and } G_3 = \frac{1}{\sqrt{2}}\begin{pmatrix}1 & -i\\ -i & 1\end{pmatrix}. \tag{42}$$

The G_1 gate manifests the bit-flip whereas G_3 is different from the standard Hadamard by a relative $\pi/2$ phase. The relative phase in G_3 can be corrected by an additional procedure by turning on the H_2 and H_3. Since these terms are diagonal, the occupation probabilities are unchanged and an appropriate time evolution can nondemolitionally correct for the phase between the qubit states. More specifically, H_3 can be used to correct the relative phase within a single qubit subspace, and H_2 corrects the overall phase of the qubit which may become important for double-qubit operations such as controlled-NOT.

The relative phase between the qubit states can be changed using the phase rotation matrix

$$G_2(\phi) = \begin{pmatrix}e^{i\,\phi} & 0\\ 0 & e^{-i\,\phi}\end{pmatrix} \tag{43}$$

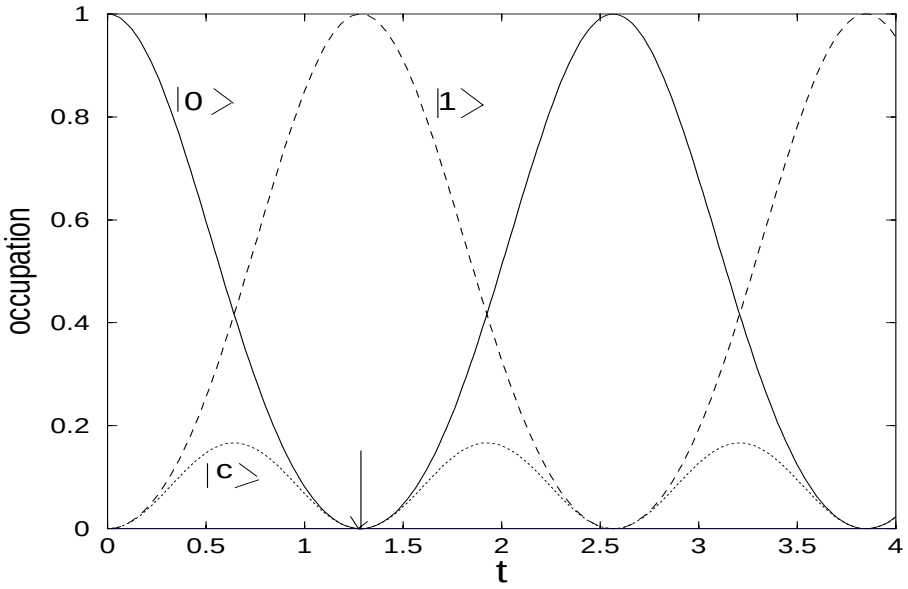

Figure 14. Evolution diagrams of quantum gate G_1. Solid and dashed lines show the time dependence of the population of the states $|0\rangle$ and $|1\rangle$ which are degenerate at $V_0 = 0$. The dotted lines show the time dependence of the auxiliary population. The arrows indicate the "operational point" of the qugate, the time of evolution corresponding to the return to the invariant qubit.

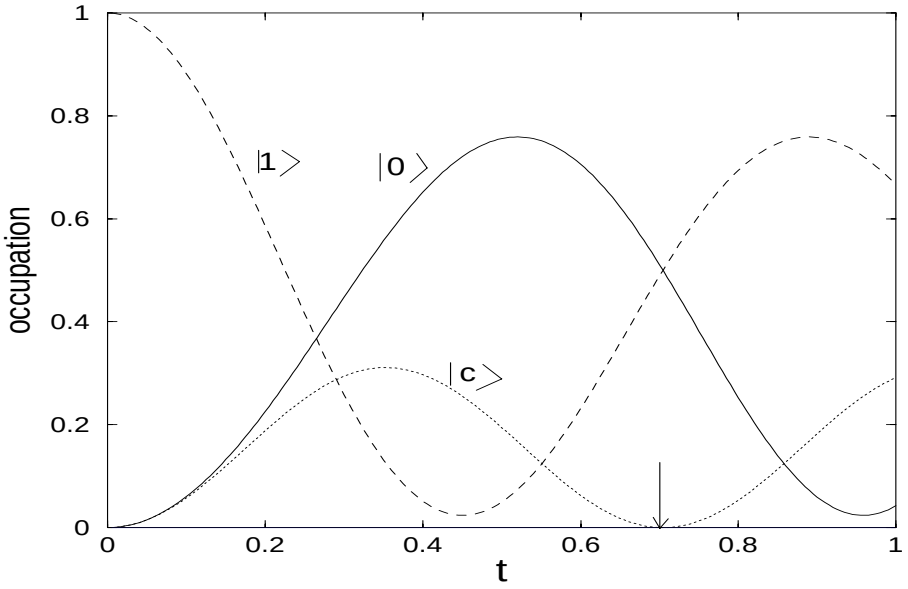

Figure 15. Evolution diagrams of quantum gate G_3. Solid and dashed lines show the time dependence of the population of the states $|0\rangle$ and $|1\rangle$ which are degenerate at $V_0 = 0$. The dotted lines show the time dependence of the auxiliary population. The arrows indicate the "operational point" of the qugate, the time of evolution corresponding to the return to the invariant qubit subspace.

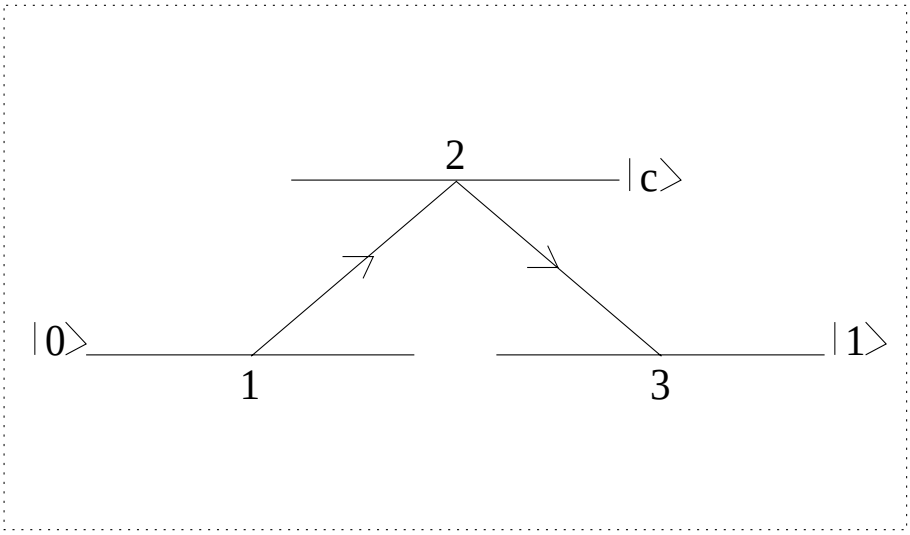

Figure 16. Λ-shaped level diagram of the persistent-current qubit. Arrows indicate the virtual transitions to the auxiliary state at the fixed-time interval (quenched) Rabi oscillation.

in the form of an Euler-type transformation $G_2(-\pi/4)\,G_3\,G_2(-\pi/4)$. The fixed phase value $-\pi/4$ can be obtained by turning off H_1 and H_2 and turning on H_3 [i.e. $H = (H_0, 0, 0, H_3)$] for the required time. Since both Hamiltonians are diagonal, the qubit subspace is invariant under this transformations for all evolution times. On the other hand, the overall qubit phase is corrected with the unitary matrix in the $H = (H_0, 0, H_2, 0)$ configuration at the fixed values $(t^*, V_0^{(*)})$ which can be easily determined.

The gate operations described in this section can be regarded as the (quenched) Rabi oscillations in a Λ-shaped level configuration of the qubit with two degenerate groundstates and one excited state (Fig.16), mostly effected by the nondiagonal matrix elements generated by H_1. In summary, the transformations between the degenerate states are achieved through a virtual transition to an auxiliary eigenstate $|c\rangle$ with a sufficiently higher energy level. Switching off the interaction, when the auxiliary state is depopulated, maps the final configuration unitarily onto the qubit subspace. The standard procedures of quantum computation are the initialization (input), the logic gate transformations in one ring, the controlled bit flips on the desired qubit pairs (the *CNOT*), and the reading of the output to a classical device.

(a)*Initialization*. Adiabatically shift the magnetic flux in each ring from half flux quantum and allow the system to relax to the nondegenerate lowest energy state $|0\rangle$ by spontaneous emission. By applying G_3, we receive a state of equally superposed degenerate levels which is conventionally the initial state in some quantum computing algorithms, in particular in the Shor's factorization algorithm [28]. In this perspective, the initialization scheme is not drastically different from other quantum computation schemes in the literature.

(b)*CNOT*. The realization of the controlled operations with double qubits is a fundamental requirement of any mechanism of quantum computation. It is possible to obtain a CNOT gate in the quantum system we propose. Two three-level systems are initially prepared to be in their qubit subspaces and they are connected by a quantum nondemolitional measurement device which reads the first qubit and depending on its state, induces a static potential $V_0^{(1)}$ in the second qubit to perform the bit flip. The experimental scheme is shown in Fig.17 which employs two mesoscopic rings, a Hall bar in the full integer quantum regime and a superconducting loop. The persistent current J_1 in the qubit $\mathbf{Q_1}$ creates a current in the superconducting loop $J_1' = \eta J_1$ by induction where η is the efficiency in the transformation of the current. The current J_1' is

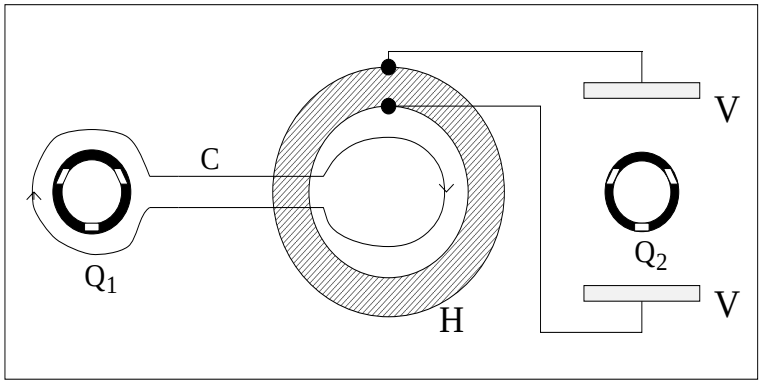

Figure 17. A sketch of the **CNOT** quantum gate. The loop of the qubit No.1 couples via the superconducting loop **C** to quantum Hall bar (**H**) in the form of a Corbino disk. The voltage output $R_{xy}J_1'$ from the disk is supplied (after subtracting a constant value V_0, not shown on figure) to potential electrodes **V** thus controlling the flip transition in the qubit No.2.

then fed into the Corbino disk and converts it to the voltage

$$V_{xy} = R_{xy}J_1' = \eta n\frac{h}{e_2}J_1 \tag{44}$$

where R_{xy} is the Hall resistance at the n'th plateau, viz. $R_{xy} = n \cdot 27k\Omega$. Here the efficiency parameter depends on the effective mutual inductance between the qubit ring $\mathbf{Q_1}$ and the superconducting loop. The reference point of the Hall voltage V_{xy} is adjusted to adopt the binary values: either $V_0^{(1)}$ or zero corresponding to the fixed value of the current flowing in one or the other direction. The Hall bar is connected to the V electrodes of qubit $\mathbf{Q_2}$. If the voltage is $V_0^{(1)}$, the bit flip of the second qubit is realized after time t_1 or if the voltage is zero no change is made. The procedure may in principle be executed in a totally reversible way provided that the Hall bar is in the manifestly quantum regime. According to the measurements [43], longitudinal currents in the contactless realization of the quantum Hall effect (the Corbino disk geometry) persist for hours, i.e. the longitudinal resistance R_{xx} practically vanishes considering the short time scales relevant for quantum computation.

(c) *Qugate operation with two coupled rings.* The objective is to implement quantum mechanically the "control-NOT" operation which flips the state of one of the two qubits (the control) provided the second (target) qubit is in one of its particular states. This means, for example, that the bit No.1 should be nondemolition-measured and, if up, the second bit is flipped. The two states $|\uparrow>$ and $|\downarrow>$ differ in the direction of their currents. We use this to design an interaction between the qubits $\hat{j}^{(1)} \otimes \hat{H}_1^{(2)}$ where $\hat{j}$ is a current operator (in proper units) $\hat{j} = diag(1, -1, 0)$ in the representation of operators A_m^+, and upper indices (1,2) correspond to the qubits No.1,2.

The realization of the controlled operations with double qubits is an essential requirement of any mechanism of quantum computation. It is possible to obtain a CNOT gate in the quantum system we propose. Both three level systems are initially prepared to be in their qubit subspaces and they are connected by a quantum nondemolitional measurement device which reads the first qubit and depending on its state, induces a static potential $V_0^{(1)}$ in the second qubit to perform the bit flip. The experimental scheme is schematized in Fig.18 which employs two mesoscopic rings, a Hall bar in the form of a Corbino disk [44] in the full quantum regime and the superconducting loop. The persistent current J_1 in the loop of qubit $\mathbf{Q_1}$ creates a current in the superconducting loop $J_1' = \eta J_1$ where η is the efficiency of current transformation

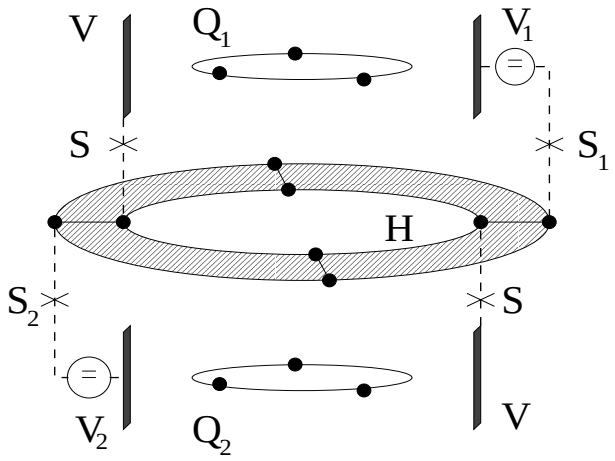

Figure 18. A sketch of the *CNOT* quantum logical gate. $\mathbf{Q_1}$, $\mathbf{Q_2}$ are qubits No.1,2, $\mathbf{V}$ are voltage electrodes and $\mathbf{V_1}$, $\mathbf{V_2}$ the voltage shift sources, $\mathbf{S_1}$, $\mathbf{S_2}$ are their respective switches. $\mathbf{H}$ is the Quantum Hall bar. Filled dots represent schematically metallic islands resonantly coupled to each other along the solid lines.

and converts it to voltage

$$V = R_{xy} J_1' = n \frac{h}{e_2} J_1' \tag{45}$$

on the center of n-th Hall plateau. The system is assumed to be initiated such that current in a loop is zero at zero persistent current in a qubit loop; the other possibility could be to include the $-\Phi_0/2$ compensating coil between $\mathbf{Q_1}$ and $\mathbf{H}$ to exclude the large static flux $\Phi_0/2$ in the qubit. Estimate shows that due to a large value of R_{xy} ($27k\Omega$ on the main Hall plateau), the voltage V is large enough to drive the qubit at the efficiency $\eta \sim 0.1$.

The Hall voltage generated in the bar is designed so that either $V_0^{(1)}$ or zero voltage is produced corresponding to the fixed value of the current flowing in one or the other direction. The Hall bar is connected to the V electrodes of qubit $\mathbf{Q_2}$. If the voltage is $V_0^{(1)}$, the bit flip of the second qubit is realized after time t_1 or if the voltage is zero no change is made. The procedure may in principle be executed in a totally reversible way if the Hall bar operates in the manifestly quantum regime.

(d)*Reading the output*. Reading the result, i.e. the population of the qubit when computation concludes can be realized with a Hall device as shown in Fig.17. Since the readout breaks the reversibility we may assume that it can also be manifested by the classical Hall effect. By measuring the magnetic field output B' from the persistent current in a loop and applying this field to a Hall bar with a large current J we receive a sufficiently large voltage $V' = R_H J B'$ the magnitude and the polarity of which reports on the magnitude and the direction of current in the qubit. This device is analogous to a Stern-Gerlach sensor of the NMR qubit in Ref.[45] , or to the Ramsey-zone measuring device of the optical beam polarization qubit in Ref.[46].

5. Discussion

We considered Aharonov-Bohm effect in angular-periodic macromolecular loop like, e.g., aromatic cyclic molecule, and found that the Aharonov-Bohm flux applied to loop arrests the lattice instability (rearrangement of molecular atoms or blocks within the molecule). This is a consequence of the fact that weak-coupling effect of electron hopping between the sites of electron localization can not provide enough energy for initiating the atoms (blocks) shifting from periodic locations, except at quite small magnetic fields. As a result,

the ground state of system at certain electron concentration becomes a current-carrying one at zero (or very small) magnetic fluxes, the state with the spontaneous persistent current. This effect suggests a possibility of using appropriately engineered macromolecular structures as elementary qubits, the degenerate or near degenerate states seeked for processing of quantum information. As was shown in a sect.IY, the three-site Aharonov-Bohm loop supports all logical operations (the quantum logical gates) required for quantum computation and quantum communication, which are effected by static voltages applied to loop perpendicular to magnetic flux and such that the loop is driven to a Λ-shaped energy configuration with the two degenerate ground states making elements of qubit, and the third, higher energy state accomplishing the radiation-free quantum logical gates. Very strong magnetic fields are required for formation of such states (corresponding to magnetic flux equal to half of flux quantum).

We proposed a new mechanism for quantum computation based on manipulation of the quantum states of the Aharonov-Bohm (non-superconducting) persistent-current states in mesoscopic (nanoscopic) loops (i.e. quantum dots; the vacancies in ionic crystals; the conducting molecular nanowires; the macromolecular aggregates). The mechanism is ultimately related to the unique property of a three-site loop, the presence of a double degenerate ground state at fixed spin orientation at the value of the Aharonov-Bohm flux in a loop equal to half of the normal-metal flux quantum. The central point is a Λ-shaped energy configuration of a three-site loop (Fig.16) with two degenerate ground states, and the existence of the unique transformations of qubit populations (Fig.14,15) accomplished with a radiation free (employing static voltages at pulse heights) external perturbations which are not subject to any *quantum* restrictions. The loop in the crossed electric and magnetic fields displays both the static (magnetic) and the dynamic (electric) Aharonov-Bohm effects and, as a result of the latter, it allows the reversible operations constituting, in their entirety, the full set of transformations expected in universal quantum computation. The estimated magnitudes of the persistent currents show that these currents, being quite small, nevertheless are in principle sufficient to operate the quantum logic gates (qugates).

The major advantage of the suggested mechanism from the currently investigated solid state (superconductive) qubits are in that, the qugate manipulations are effected by static pulsed voltages in a totally radiation free environment. Namely, no external coupling to a resonant laser field is necessary.]In the proposed mechanism, the decoherence may be further reduced effectively by the fact that the qubit and the qugate, being a single unit, optimize the adiabatic evolution by minimizing the number of external switches required. Add to this that certain estimates [24] conclude on the quite small decoherence effects, at appropriate choice of the system parameters, related to the qubit interaction with a radiative environment.

It is very likely that the simplicity of the theoretical mechanism and the flexibility in the conducting molecular structures may also permit persistent current states. Some difficult parts of the scheme (the requirement of quite strong magnetic fields to operate the qubit; the low level of electromagnetic signals in the loops; the severe limitation on precision of voltage amplitude and time duration in logical gates; the low temperature environment needed to enter the regime when the persistent current becomes a non-exponentially small effect) may be overcome by a due extension of the model. These issues are not discussed in present paper in any practical detail except of mentioning that spontaneous persistent currents discussed in sect.III allow to reduce these fields by orders of magnitude. If not the goal of building a real quantum computer, the very existence of the nonzero persistent currents at vanishingly small magnetic fields deserves, to our opinion, a basic physical interest.

References

[1] F. Bloch, *Phys. Rev.*, **B2**, (1970), 109 and references therein. This paper proved exact periodicity of energy in one dimensional ring as a function of magnetic flux with a period hc/e, however with the indefinite amplitude.

[2] I.O. Kulik, *Pis'ma Zh. Eks. Teor. Fiz.,* **11**,(1970), 407, [*JETP Lett.,* **11**, (1970), 275].

[3] Y. Aharonov and D. Bohm, *Phys. Rev.*, **115**, (1959), 485.

[4] M. Buttiker, Y. Imry and R. Landauer, *Phys. Lett.,* **A96**, (1983), 365.

[5] V. Chandrasekhar, R.A. Webb, M.J. Brady, M.B. Ketchen, W. J. Gallagher and A. Kleinsasser, *Phys. Rev. Lett.,* **67**, 3578 (1991).

[6] D. Mally, C. Chapelier and A. Benoit, *Phys. Rev. Lett.,* **70**, 2020 (1993).

[7] D. Gatteschi, A. Caneschi, L. Pardi, and R. Sessoli, Science **265**, 1054 (1994); K.L. Taft, C.D. Delfs, G.C. Papaefthymiou, S. Foner, D. Gatteschi, and S.J. Lippard, *J. Amer. Chem. Soc.*, **116**, (1994), 823.

[8] A. Barone, T. Hakioglu and I.O. Kulik, *Quantum Computation with Aharonov-Bohm Qubits*. E-print cond-mat/0203038 (2002).

[9] I.O. Kulik, *Quantum bistability, Peierls transition, and spontaneous persistent currents in mesoscopic Aharonov-Bohm loops*, submitted to Phys. Rev. Lett.

[10] E. Teller, *Zs. Physik*, **67**, (1931), 311.

[11] M. van Leeuwen, *J. Phys.*, **2**, (1921), 361.

[12] I.M. Lifshitz, M. Ya. Azbel, and M.I. Kaganov, *Electron Theory of Metals*, Nauka Publ., Moscow, 1971.

[13] L.D. Landau, *Zs. Physik,* **64**, (1930), 629.

[14] I.O. Kulik, Non-decaying currents in normal metals, in: *Quantum Mesoscopic Phenomena and Mesoscopic Devices in Microelectronics*, p.259, ed. I.O. Kulik and R. Ellialtioglu, Kluwer, 2000.

[15] J. Bardeen, L.N. Cooper, and J.R. Schrieffer, **108**, (1957), 1175.

[16] H.F. Cheung, E.K. Riedel, and Y. Gefen, *Phys. Rev. Lett.,* **62**, (1989), 587.

[17] I.O. Kulik and I.K. Yanson, *The Josephson Effect in Superconductive Tunneling Structures*, Israel Program for Scientific Translations, Jerusalem, 1972.

[18] A. Barone and G. Paterno, *Physics and Applications of the Josephson Effect*. J. Wiley, NY, 1982.

[19] A.J. Leggett, in: *Chance and Matter*, p.395. Ed. J. Souletier, J. Vannimenus, and R. Stora, Elsevier, Amsterdam, 1996.

[20] K.K. Likharev, *Dynamics of Josephson Junctions and Circuits*. Gordon and Breach Publ., Amsterdam, 1996.

[21] Y. Makhlin, G. Schön, and A. Schnirman, Rev. Mod. Phys. **73**, (2001), 357.

[22] N.B. Brandt, E.N. Bogachek, D.V. Gitsu, G.A. Gogadze, I.O. Kulik, A.A. Nikolaeva, and Ya. G. Ponomarev, *Fiz. Nizk. Temp.* **8**, (1982), 718, [*Sov. J. Low Temp. Phys.,* **8**, (1982), 358].

[23] L.P. Levy, G. Dolan, J. Dunsmuir, and H. Bouchiat, *Phys. Rev. Lett.,* **64**, (1990), 2074.

[24] I.O. Kulik, T. Hakioglu, and A. Barone, *Eur. Phys. J. B*, **30**, (2002), 219.

[25] I. O. Kulik, Quantum Computation with Aharonov-Bohm Qubits, in: *Towards the Controllable Quantum States: Mesoscopic superconductivity and spintronics*, ed. H. Takayanagi and J. Nitta. World Scientific, 2002.

[26] I. O. Kulik, ABC: A double-conversion compiler/solver for nanoscience calculus, in: *Techn. Proc. of 2003 Nanotechnology Conference and Tradeshow*, vol.**2**, p.531. Eds. M. Laudon and B. Romanowicz, Computational Publications, Boston, 2003.

[27] M. A. Nielsen and I. L. Chuang, *Quantum Computation and Quantum Information*. Cambridge Univ. Press, 2000.

[28] P. W. Shor, in: Proc. 35th Annual Symp. Th. Comp. Science, p.124. Ed. S. Goldwasser, IEEE Comp. Soc. Press, Los Alamos, 1994.

[29] D. Loss and D.P. DiVincenzo, *Phys. Rev.*, **A57**, (1998), 120.

[30] Y. Nakamura, C.D. Chen, and J.S. Tsai, *Phys. Rev. Lett.,* **79**, (1997), 2328.

[31] A. Shnirman, G. Schön, and Z.Hermon, *Phys. Rev. Lett.*, **79**, (1997), 2371.

[32] Y. Makhlin, G, Schön, and A. Shnirman, *Nature*, **398**, (1999), 305.

[33] V. Bouchiat, D. Vion, P. Joyez, D. Esteve, and M.H. Devoret, Phys. Scripta **T76**, 165 (1998).

[34] T.P. Orlando, J.E. Mooij, Lin Tian, C.H. van der Wal, L.S. Levitov, S. Lloyd, and J.J. Mazo, *Phys. Rev.,* **B60**, (1999), 15398; *Science*, **285**, (1999), 1036.

[35] L.V. Ioffe, V.B. Geshkenbein, M.V. Feigelman, A.L. Fauchere, and G. Blatter, *Nature*, **398**, (1999), 679.

[36] A.M. Zagoskin, "A scalable, tunable qubit, based on a clean DND or grain boundary D-D junction", e-print cond-mat/9903170.

[37] D.D.P. Di Vincenzo, G. Burkard, D. Loss, and E.V. Sukhorukov, "Quantum computation and spin electronics", in: Quantum Mesoscopic Phenomena and Mesoscopic Devices in Microelectronics, p.399. Eds. I. O. Kulik and R. Ellialtioglu. Kluwer, Dordrecht, 2000.

[38] Y. Makhlin, G. Schön, and A. Shnirman, *Rev. Mod. Phys.,* **73**, (2001), 357.

[39] D.V. Averin, *Solid St. Commun.*, **105**, (1998), 659.

[40] C. Kittel, *Introduction to Solid State Physics*, J. Wiley, NY, 1996.

[41] S. Iijima, *Nature (London)*, **354**, (1991), 56.

[42] S. Ciraci, A. Buldum and I. Batra, *J. Phys: Condens. Matter*, **13**, (2001), R537.

[43] V.T. Dolgopolov, A.A. Shashkin, N.B. Zhitenev, S.I. Dorozhkin, and K. von Klitzing, *Phys. Rev.,* **B46**, (1992), 12560.

[44] S. Das Sarma and A. Pinczuk, *Perspectives in Quantum Hall Effects*, Wiley, 1996.

[45] A. Barenco, *Contemp. Phys.,* **37**, (1996), 375.

[46] C.H. Bennett, Phys. Today, p.24, Oct.1995.